LANGMUIR

pubs.acs.org/Langmuir Article

Long-Term Static and Dynamic Corrosion Stability of Nonwetting Surfaces

S.M.A. Mousavi and R. Pitchumani*

Cite This: *Langmuir* 2022, 38, 6911−6922 Read Online

ACCESS | Metrics & More | Article Recommendations

ABSTRACT: Superhydrophobic surfaces (SHSs) and lubricant-infused surfaces (LISs) are two classes of nonwetting surfaces that have drawn attention due to their advanced functional properties including corrosion inhibition. Yet there is a conspicuous lack of corrosion study of SHSs and LISs with respect to their fabrication and material parameters, especially at high temperatures and under dynamic flow conditions over long durations, which is sought to be addressed in this article. Considering copper SHSs and LISs, a full factorial combinatorial study of two facile texturing processes, electrodeposition and etching, two different functionalization agents, stearic acid and mercaptan, and two types of infused lubricants, Krytox 104 and DOWSIL 510, is presented, encompassing over 650 measurements on 90 tested surfaces. All fabricated surfaces demonstrated water repellency with a contact angle above 150° and a sliding angle below 7°. For the first time, the study examines high-temperature corrosion stability and long-term corrosion durability of the nonwetting surfaces in both static fluid and dynamic turbulent flow conditions over a period of 30 days. LISs and SHSs are shown to provide excellent corrosion inhibition over all tested corrosion conditions, with negligible presence of corrosion species on the surfaces and no deterioration of the texturing. The surfaces are also shown to rejuvenate easily to the initial wettability and corrosion resistance values. This study provides valuable insights into the selection of materials and processing parameters for the fabrication of nonwetting surfaces for the application of interest.

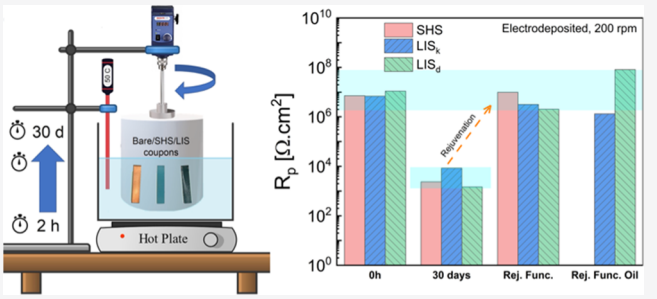

1. INTRODUCTION

Surface wettability has a huge impact on our everyday experience, from printing inks to the waxy coating used to protect cars. Throughout the years and for different purposes, the wetting, spreading, adhesion, and dewetting of a liquid on a solid have been optimized.[1] Some applications include adhesion of paint to surfaces, anti-fouling coatings for marine constructions,[2,3] stain-resistant appliances,[4−6] and anti-icing surfaces in the aviation sector.[7] Also, self-cleaning metallic materials were widely explored for the reduction of biofouling,[8,9] mineral scaling,[10,11] and corrosion.[12−15] The need for anti-fouling metallic surfaces naturally arises from their broad usage. For example, one of the hefty and costly problems for industries around the world is the direct and indirect cost of corrosion of metallic surfaces that equals 3−5% of the global gross national product.[16,17]

Metallic surfaces, including copper, are omnipresent in condensers and evaporators of refrigerators or air conditioners, in power plant heat exchangers, and in the marine industry. Therefore, corrosion inhibition of copper surfaces has been the center of attention and is improved via various methods.[12,18] Adsorption of species, including corrosive ions, on a surface, can theoretically be prevented by reducing the wetted solid−electrolyte contact area and, in turn, mitigating different types of fouling, including corrosion.[19] Pursuant to that concept and inspired by *lotus* leaf and *Nepenthes* pitcher plant, two classes of nonwetting surfaces—superhydrophobic surfaces (SHSs) and lubricant-infused surfaces (LISs)—have been explored to mitigate fouling, including corrosion. SHS, with a high contact angle (CA) above 150° and a low roll-off angle below 10°, provides an air cushion between the electrolyte and surface[12] and, similarly, LIS, incorporating a slippery lubricated layer with a sliding angle below 10°, provides protection against fouling.[15]

Wang et al. fabricated liquid-infused aluminum to ease the adherence of sulfate-reducing bacteria in a static seawater condition.[20] Song et al.[21] textured the aluminum substrate by electrochemically anodizing with ordered pores of several tens of nanometers and further transformed it into a LIS by immersing the surface in methyl silicone oil, fluoroalkyl silane,

Received: February 9, 2022
Revised: May 8, 2022
Published: May 25, 2022

https://doi.org/10.1021/acs.langmuir.2c00331
Langmuir 2022, 38, 6911−6922

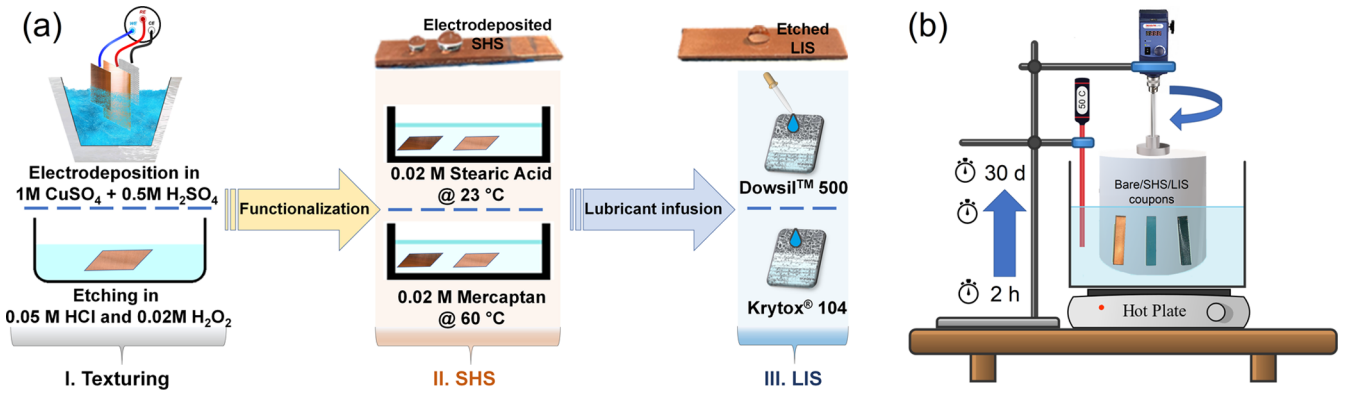

Figure 1. Schematic illustration of the (a) steps in the fabrication of superhydrophobic and lubricant-infused nonwetting surfaces and (b) dynamic corrosion setup depicting metallic coupons mounted on the outer surface of the inner rotating drum in a stationary cylindrical tank filled with corrosive solution containing 3.5% sodium chloride.

and finally Krytox 104 oil, which demonstrated excellent anti-corrosion properties in a 3.5% saline solution at low temperature. Shi et al.[22] dealloyed CuZn in a $CuSO_4$ bath, later added dodecanethiol by a chemical vapor deposition process, and finally infused the surface with perfluorinated lubricant for corrosion study in seawater of 3% salinity. They reported up to 2 orders of magnitude lower corrosion current density compared to bare CuZn at room temperature. Xiang et al.[23] coated mild steel with ZnNi via electroplating at 4 $A{\cdot}dm^{-2}$ at 35 °C for 20 min. After that, the samples were immersed in fluoroalkyl silane solution and then lubricated with Krytox 100 oil. The corrosion behavior of the samples was studied in a 3.5 wt. % NaCl solution at room temperature. The mild steel LIS was reported to show about 3 orders of magnitude reduction in corrosion current compared to bare iron. Qiu et al.[24] reported on grown micro/nanoscale copper via electrodeposition for 10 min at −1000 mV on Cu/Al and Al/Mg alloys and used it as a catalyzer for growing carbon fibers. To develop hydrophobic carbon fibers, the textured substrates were placed in a tube furnace at 350 °C in an acetylene gas flow and further impregnated with a lubricant. In a 3.5% NaCl solution at room temperature, the LIS had a higher corrosion impedance than the hydrophobic surface without liquid infusion.

In general, fabrication of SHSs requires two steps of texturing and applying a functional group to the surface to reduce the surface energy, while LISs are fabricated in three steps: texturing, functionalization, and lubricant impregnation. Several reviews have been dedicated to SHS and LIS fabrication as well as specific applications.[25,26] Texturing can be accomplished by processes that fall into one of the two categories, *additive* or *removal* methods,[27] and include templating, sol−gel method,[18,28] electrospinning,[29] laser etching,[30] hydrothermal synthesis,[31] anodization, plasma techniques,[32] and electrodeposition.[26,33] LIS fabrication studies in the literature have focused on two main classes of infused lubricants: perfluoropolyethers (PFPEs) and linear polydimethylsiloxane (PDMS), also known as silicone oil or dimethicone.[34] Several studies in the literature have investigated the corrosion inhibition property of SHSs and LISs in static[35−37] or laminar flow condition at a single temperature.[10,18,38] These studies, however, do not translate to the performance of the surfaces when the environment of application is turbulent or varies with temperature, especially over long exposure durations.

Despite the large volume of literature on nonwetting surfaces, there is a conspicuous lack of study of long-term durability and performance of SHSs and LISs in corrosive application environments, especially those involving dynamic turbulent flow conditions and elevated temperatures. Indeed, these are highlighted as areas of critical research need in recent review articles.[25,34,39] Toward addressing the knowledge gap, this article offers a comprehensive study of long-term durability of both SHS and LIS in a corrosive marine environment. Two facile texturing processes were considered, one from each of *additive* and *removal* methods, and two different functionalization agents were selected, along with two types of infused lubricants, one from the PFPE group and the other from the PDMS group. The nonwetting surfaces were created on copper, as a representative metal, for its ubiquity in applications.

Through an extensive suite of parametric tests, the effects of surface texture, functionalization material, and infused lubricant on the corrosion inhibition performance of the as-fabricated SHS and LIS along with the bare copper control sample in 3.5% NaCl solution are studied. For the first time, the study assesses the corrosion stability of the surfaces at high temperature and the long-term corrosion inhibition durability of the nonwetting surfaces in both static fluid and dynamic turbulent flow conditions in a cylindrical Taylor−Couette flow setup. For the various combinations of materials and testing conditions, long-term corrosion stability was investigated over a period of 30 days, with data collected at several interim time intervals. The corrosion inhibition properties were measured using electrochemical methods, which provide more accurate characterization in contrast to the gravimetric method that is often used in the literature, which suffers from lack of precision, especially considering lubricant or material loss in SHS and LIS vis-à-vis corrosion mass gain. On the whole, this study not only offers facile methods for the fabrication of advanced functional nonwetting surfaces but also with 90 coupons and over 650 measurements provides for the first time a comprehensive understanding of SHS and LIS by juxtaposing a rational selection of texturing methods, functionalization agents, and lubricant combinations that are subjected to tests under static and dynamic conditions at different temperatures.

2. EXPERIMENTAL METHODS

2.1. Materials and Reagents. Plain multipurpose copper sheet was purchased from McMaster, USA. Sulfuric acid (H_2SO_4),

https://doi.org/10.1021/acs.langmuir.2c00331
Langmuir 2022, 38, 6911−6922

hydrochloric acid (HCl), analytical grade copper sulfate ($CuSO_4$, 99+%), acetone (99.5+%), methanol (99.8+%), iron(III) chloride (98%), and stearic acid ($CH_3(CH_2)_{16}CO_2H$, 97%) were purchased from Fisher Scientific (Pittsburgh, PA, USA) and used as received without any further purification. Deionized (DI) water (14 MΩ·cm resistance) was purchased from CQ Concept (Illinois, USA). Hydrogen peroxide solution (H_2O_2) was purchased from Sigma-Aldrich (St. Louis, Missouri, USA). Krytox 104 silicon lubricant was purchased from Miller-Stephenson Chemical Co. (Danbury, Connecticut, USA), and DOWSIL 510 fluid was purchased from DuPont (Wilmington, Delaware, USA).

2.2. Fabrication of SHSs and LISs. The steps in the fabrication of SHSs and LISs are depicted schematically in Figure 1a. Surface texturing is the first step in the fabrication of nonwetting surfaces that was accomplished using two methods: chemical etching, a material *removal* method, and electrodeposition, an *additive* method. The as-received copper sheet was cut into coupons of 1 × 3 cm, which were degreased in a sonication bath of methanol, acetone, and DI water for 10 min each, sequentially. In the material *removal* method, the roughness features were carved into the surface via chemical etching in an aqueous solution of 0.02 M hydrochloric acid and 0.05 M hydroperoxide [6:25:19 v/v/v mixture of DI water/H_2O_2 (3%)/HCl (12 M)]. The cleaned and cut coupons were submerged in the etchant solution for 20 min.

In the additive method, multiscale asperities were grown on top of the copper surface by a three-electrode, two-step *electrodeposition* process[12] using an AUTOLAB PGSTAT128N electrochemical station (ECO Chemie, Utrecht, The Netherlands). A platinum mesh was used as the counter electrode and a copper sheet served as the reference electrode. A deaerated aqueous solution of 1 M $CuSO_4$ and 0.5 M H_2SO_4 was used as the electrolyte. The two-step electrodeposition process was initiated by applying −1.1 V for 5 min to the copper sample as the working electrode, followed by 10 s electrodeposition at −0.15 V as the second step. The second deposition served to further stabilize the first coating onto the surface. The electrodeposition process involves the reduction of copper cations to the solid copper deposited on the surface per $Cu^{2+} + 2e^- \rightarrow Cu$. Therefore, assuming a uniform coating, the deposition thickness is calculated as $h = QM/nF\rho A$, where Q is the charge transferred in coulomb throughout the deposition ($Q = i \cdot dt$), M is the molar weight of copper, n is the number of transferred electrons in the copper reduction reaction, F is the Faraday constant, A is the surface area of the deposition, and ρ is the density of the deposited copper. Accordingly, 5 min of first-stage electrodeposition was chosen to produce a coating with about 30 μm thickness.

Thereafter, the coupons fabricated via both electrodeposition and etching methods were rinsed with a copious amount of DI water and stored in a vacuum oven at 110 °C overnight to dry. Alternatively, the samples may be air-dried to achieve the same result. Furthermore, the textured surfaces were functionalized by immersion in 0.02 mol/L of stearic acid−methanol solution at room temperature or 0.02 mol/L mercaptan−ethanol solution at 60 °C for durations ranging from 1 h to 24 h. The chemisorption of the functionalization agent reduces the surface energy of the textured surfaces to form SHSs.

The as-fabricated SHS bears the appropriate surface chemistry to host a lubricant in the interasperity crevices. LISs were fabricated by infusing the SHS with lubricant oils—DOWSIL fluid (reported viscosity 500 cSt at 25 °C) or Krytox 104 (reported viscosity 177 cSt at 20 °C[34] and 60 cSt at 40 °C)—that are selected to be immiscible with the contacting brine solution in the corrosion tests. Drops of either lubricant were placed onto the SHS, and the coupons were hung vertically for at least 20 min to allow the lubricant to wick into the interasperity porous structures and to drain any surplus oil. The initial lubricant thickness in the electrodeposited LIS was measured using laser confocal microscopy to be ∼22 μm.[15]

As a matter of notation throughout the article, the superhydrophobic surfaces are referred to as SHSs, while the lubricant-infused surfaces are denoted as LISs. Superscript "D" or "E" is used to identify the texturing method as either electrodeposition or etching, respectively. For LISs, subscript "d" or "k" refers to the infused lubricant as either DOWSIL or Krytox.

2.3. Morphology and Wettability Characterization. A stylus profilometer (Dektak XT Bruker, Massachusetts, USA) with a 2 μm radius stylus tip and a working force of 10 mg and a 0.1 μm scan resolution was utilized to evaluate the surface roughness. Three-dimensional reconstruction of the surfaces was achieved using a white light scanning confocal microscope (Keyence model VK-X, Osaka, Japan). A field-emission scanning electron microscope (LEO/Zeiss 1550, Germany) equipped with an energy-dispersive X-ray (EDX) spectrometer (Oxford, UK) was used to highlight the surface morphology and chemical composition working at an acceleration voltage of 20 kV. The optical picture of the surfaces was taken using a Nikon Eclipse LV100ND Microscope with an epifluorescence filter (Nikon Instruments Inc., Japan). A goniometer (ramé-hart model 590, New Jersey, USA) was used to measure the surface wettability in terms of water contact and roll-off/sliding angle on the surfaces. A 10 μL sessile DI water droplet was placed at five different locations on each sample to calculate the average CA and the error bar (standard deviation) about it. The sliding/roll-off angle was recorded via the tilting cradle method as the angle at which a 25 μL DI water droplet rolls of an SHS. The sliding angle for a droplet on an LIS was recorded when both the rear and front contact lines of the droplet started to slide.

2.4. Dynamic Corrosion Characterization. Dynamic corrosion was studied using an annular Taylor−Couette flow[40] setup in which a rotating cylindrical drum of radius 10 cm was placed concentric inside an outer stationary cylindrical tank of radius 18 cm, as depicted in Figure 1b. The rotation of the inner drum was driven by a motor with a vertical shaft, such that the rotational speed can be set to desired values. The annulus between the inner cylindrical drum and the outer cylindrical tank was filled with corrosive solution containing 3.5% sodium chloride mimicking a marine environment. The test coupons were mounted on the outer surface of the inner drum such that they experienced a dynamic shear due to the rotational fluid flow in the annulus. The setup was placed on a hot plate so that the solution can be heated to a desired temperature, measured using a thermometer with a digital readout, and immersed in the solution in the annulus. A feedback control loop was used to control the hot plate to achieve a set point temperature of the corrosive solution.

Corrosion experiments were conducted on superhydrophobic and lubricant-infused copper surfaces fabricated by electrodeposition and etching at rotation rates, Ω, of 0 rpm (for static corrosion studies) and 200 rpm (for dynamic corrosion studies) and temperatures of 23 and 70 °C. In addition, for reference, dynamic fouling studies were also conducted on bare copper coupons at the two rotational speeds and the two temperature values. In each case, to understand the time evolution of corrosion, coupons were removed at time durations of 2 h, 4 h, 8 h, 1 day, 4 days, 8 days, 12 days, 15 days, 20 days, 25 days, and 30 days from the start of the experiment, as depicted in Figure 1b. Three replicates were analyzed at each parametric combination of surface type, rotation speed, temperature, and time duration for a total of 90 coupons and over 650 measurements in the overall experimental matrix.

To assess the corrosion inhibition of the samples, three-electrode (reference, counter, and working electrodes) electrochemical tests were performed. As a reference electrode, Ag/AgCl (NaCl saturated) was placed at less than 3 mm distance from the sample surface (working electrode) to minimize the solution resistance interference in the measurement. A counter electrode made of platinum mesh was placed equidistant from the other two electrodes. A potentiostat device, Solartron Inc. (model 1240 PA, USA), was used to record potentiodynamic polarization (PDP) curves and linear polarization (LP) test data. After 40 min of immersion in corrosive solution, PDP curves were scanned from −300 to +300 mV with respect to the open circuit potential. After 5 min of stabilization, LP tests were scanned in the range of −20 to +20 mV. Per ASTM G3-14,[41] scan rates of 1 mV/s and 1/6 V/h were used for the PDP and LP tests, respectively.

The PDP curve and the LP scan from corrosion tests were further reduced to corrosion rate and polarization resistance, respectively. A

https://doi.org/10.1021/acs.langmuir.2c00331
Langmuir 2022, 38, 6911−6922

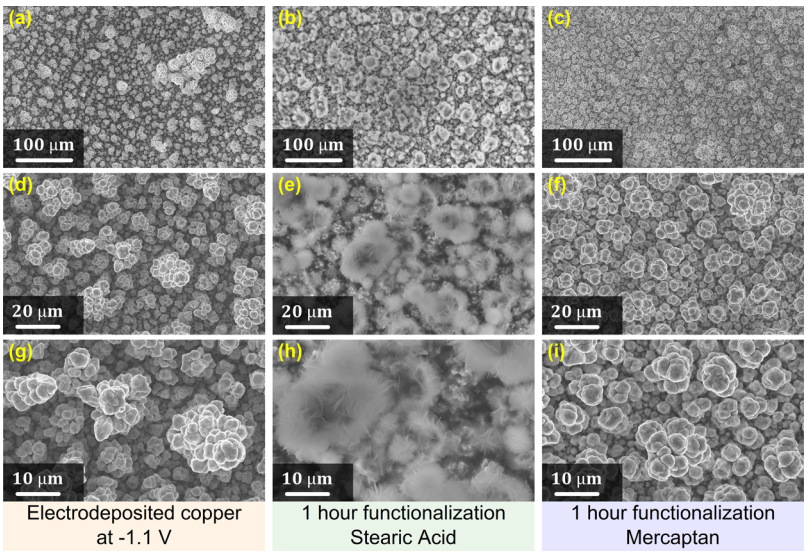

Figure 2. SEM images of the (a,d,g) as-fabricated electrodeposited copper surface; (b,e,h) electrodeposited copper surface after 1 h of stearic acid functionalization; and (c,f,i) electrodeposited copper surface after 1 h of mercaptan functionalization.

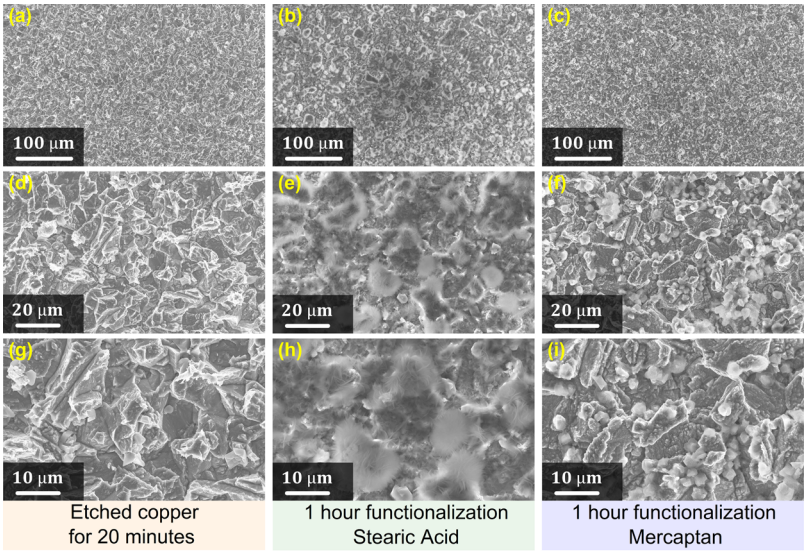

Figure 3. SEM images of the (a,d,g) as-fabricated etched copper surface; (b,e,h) etched copper surface after 1 h of stearic acid functionalization; and (c,f,i) etched copper surface after 1 h of mercaptan functionalization.

Tafel extrapolation approach was utilized to quantitatively determine the corrosion parameters from the measured PDP data. The PDP test data was plotted in a semi-log current (j)−voltage (V) space to obtain the Tafel plot, from which the corrosion current density (j_c) is obtained as the intersection of the asymptotes to the cathodic and anodic regions of the Tafel plot. The corrosion rate (CR) in mm/year (mmPY) was then calculated as CR = $3276.6 j_c \cdot EW/\rho$, where ρ is the metal density and EW is the equivalent weight defined as A_w/nF, in which A_w is the atomic weight, F is the Faraday constant, and n is the number of electrons transferred per metal atom, according to the anodic corrosion reaction: $M \rightarrow M^{n+} + n \cdot e^-$. The LP potential−current density profile from the LP scan data was used to calculate the corrosion potential (E_c) as the intersection of the $j = 0$ line and the scanned $j-V$ profile. The polarization resistance, R_p, was, in turn, recorded as the slope of a linear fit at ±10 mV around E_c on the LP profile. For each experimental condition, the corrosion rate was measured on three replicates of the samples, from which an average and standard deviation were determined. The standard deviation is shown as the error bar around the average value in the data presented and discussed in the next section.

3. RESULTS AND DISCUSSION

In this section, the findings of the study are presented, where first the morphology and surface characterization of the as-fabricated SHS and LIS are discussed (Section 3.1), followed by the high-temperature stability of the fabricated nonwetting surfaces (Section 3.2). Systematic, long-term static and dynamic corrosion studies of the as-fabricated nonwetting surfaces along with the bare copper control surface are discussed in Sections 3.3 and 3.4, respectively, and rejuvenation of the nonwetting characteristics of the surfaces following corrosion is discussed in Section 3.5.

3.1. Morphology and Wettability. The scanning electron microscope (SEM) images shown in Figure 2 elucidate the morphology of the electrodeposited copper surfaces. In the electrodeposition process, copper is added on the surface of the copper substrate to form a forest of micro- and macro-sized features as shown in the lower magnification image of Figure 2a. The progressively higher magnification images of the

https://doi.org/10.1021/acs.langmuir.2c00331
Langmuir 2022, 38, 6911−6922

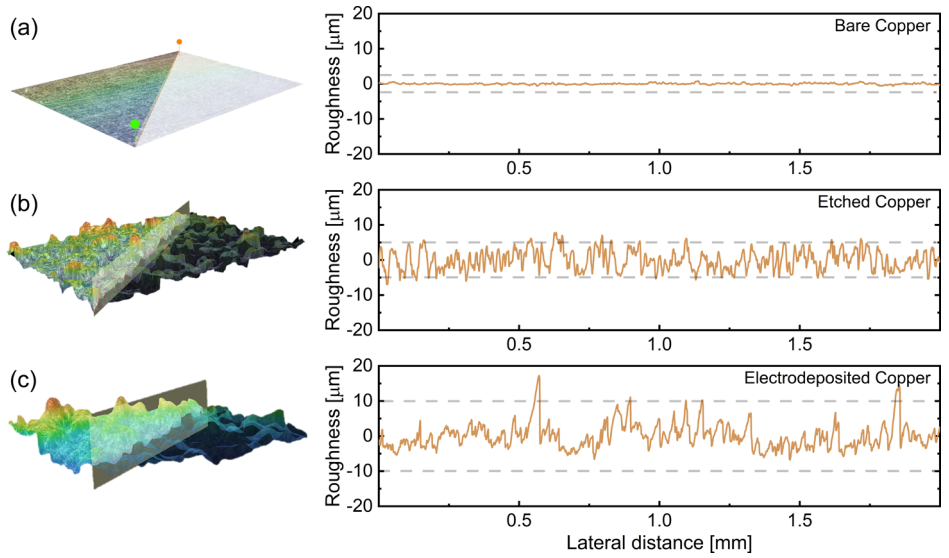

Figure 4. Three-dimensional surface reconstruction and roughness profile of (a) bare, (b) etched, and (c) electrodeposited copper surfaces.

unfunctionalized electrodeposited copper surface shown in Figure 2d,g reveal cauliflower-shaped multiscale features, where the florets range in size from small at the bottom to large at the top, Figure 2a,d,g. The multiscale features are characterized by a fractal dimension as high as 1.90[42,43] and result in deep asperity trenches on the surface. After functionalization in stearic acid solution for 1 h, the chemisorbed fatty acid covers first the top cauliflowers in the form of nanoscale cabbage-leaf-like features, Figure 2b, and covers the smaller dimension flowers at the bottom in the form of a nanoscale-thick sheath, Figure 2e,h. Our previous study[12] explored the chemical composition of the stearic acid functionalization layer through detailed XPS analysis to show the chemisorption of stearic acid (rather than physisorption) onto the copper surface. No adsorbed material was seen in the form of crystals (either to the naked eye or via SEM). Moreover, XRD analysis, which works on the principle of diffraction in the crystal lattice, showed no meaningful signature in its spectra, suggesting an amorphous, rather than a crystal structure. Unlike stearic acid functionalization, functionalization with mercaptan leads to a thin conformal coating on the as-electrodeposited textures and does not add any significant new morphological features as can be seen in Figure 2c,f,i.

Following a similar format as shown in Figure 2, the surface morphology of etched surfaces before functionalization is depicted in Figure 3a,d,g at different magnifications, where the random roughness that is introduced into the surface via the etching process is clearly shown. The structures also exhibit a multiscale morphology with a fractal dimension of up to 1.80.[42,43] The effect of functionalization on the morphology was found to be similar for electrodeposited and etched surfaces. Functionalization of the etched surface in stearic acid solution for 1 h, Figure 3b,e,h, results in a cabbage-like morphology on the surface, whereas 1 h of functionalization with mercaptan, Figure 3c,f,i, results in a conformal thin coating that tightly contours the as-deposited etched texture.

The surface topography of the bare and textured surfaces was examined with a profilometer. Figure 4a depicts a three-dimensional reconstruction of a bare copper surface along with its roughness profile, demonstrating the smoothness of the surface with the profile height smaller than 1 μm. Figure 4b shows that surface texturing via chemical etching results in a homogeneous random profile with a peak-to-valley height of ~12 μm. In contrast, the electrodeposition method of texturing yields a relatively inhomogeneous random profile with a higher peak-to-valley height of ~29 μm, as can be seen in Figure 4c. The electrodeposited surface roughness profile can be distinguished into two levels: the base flower farm and the grown cauliflowers protruded above the base (as shown in Figure 2d). In that perspective, Figure 4c shows a homogeneous first-level random base roughness within the ±10 μm range interspersed with taller, second-level, features in the range of ±20 μm.

The surface roughness measures of the different surfaces through the various stages of fabrication are summarized in Table 1 in terms of the root-mean-squared (RMS) roughness and the peak-to-valley height. It is evident that the textured surfaces via etching or electrodeposition have greater roughness compared to bare copper. For the etched textured surfaces, functionalization in either stearic acid or mercaptan has relatively less effect on the surface roughness. For electrodeposited textured surfaces, functionalization with stearic acid shows a rather substantial increase in the roughness of the surface. This is attributed to the aggressive texturing via electrodeposition, which presents abundant sites for chemisorption and growth of the cabbage-like stearic acid features,

Table 1. Calculated Surface Roughness Properties from Profilometry Scans

surface	RMS roughness (μm)	peak-to-valley height (μm)
bare copper	0.15	0.69
etched copper	2.92	12.84
electrodeposited copper	3.72	29.82
etched, stearic acid functionalized	2.40	11.84
electrodeposited, stearic acid functionalized	6.90	49.12
etched, mercaptan functionalized	1.84	13.33
electrodeposited, mercaptan functionalized	4.08	28.06

https://doi.org/10.1021/acs.langmuir.2c00331
Langmuir 2022, 38, 6911−6922

therefore further increased the roughness with higher height asperities. In contrast, mercaptan coating simply conforms to the textured electrodeposited surfaces and does not lead to any additional roughness, as can be seen in Table 1.

A consequence of texturing and functionalizing the etched and electrodeposited surfaces is their nonwetting characteristic, described in terms of the water CA and the sliding angle (roll-off angle for SHS) presented in Figure 5 for the different

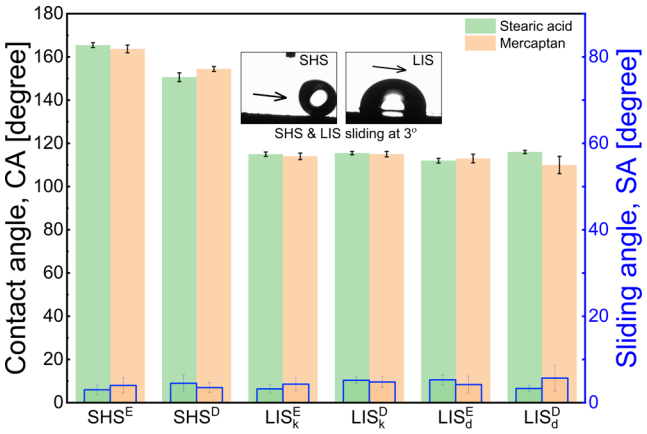

Figure 5. Water CA and roll-off/sliding angle on the fabricated superhydrophobic copper surfaces (SHSs) and lubricant-infused copper surfaces (LISs). Inset shadowgraphs show a 25 μL droplet rolling off an SHS^D and sliding off an electrodeposited surface functionalized with stearic acid and infused with DOWSIL (LIS^D_d) at a 3° cradle tilt.

textured and LISs. The surfaces were functionalized for 24 h. As can be seen, all the etched and electrodeposited surfaces, regardless of the functionalization agent, exhibit an average water CA above 150° and a low roll-off angle below about 7°, demonstrating superhydrophobicity. Slipperiness of the etched as well as electrodeposited LIS, infused with either Krytox 104 or DOWSIL, is uniformly evident with the sliding angle < 7° for both functionalization agents. For LISs, the water CA is about 110°, consistent with the values reported in the literature. The inset shadowgraphs in Figure 5 show a 25 μL droplet rolling off an electrodeposited superhydrophobic surface (SHS^D) and sliding of an electrodeposited surface that is functionalized with stearic acid and lubricated with DOWSIL (LIS^D_d) at only a 3° cradle tilt.

3.2. High-Temperature Corrosion Stability. Prior to conducting the long-term corrosion studies, the corrosion stability of the fabricated surfaces with temperature was examined by immersion in 3.5% NaCl solution at T_i = 23 and 70 °C. The measured CR of the different nonwetting surfaces functionalized with stearic acid and mercaptan for 24 h are shown in Figure 6a,b, respectively. In each plot, the data is organized by the texturing method and shows the comparison of SHSs and LISs with the two different infused lubricants. For reference, the corrosion rate of the bare copper surface at the two temperatures is shown by the dashed lines in each plot.

For SHS, at T_i = 23 °C, the corrosion rate values of the electrodeposited SHS are seen to be lower than that for the etched SHS, for both stearic acid and mercaptan functionalizations. Among the stearic acid functionalized SHSs (Figure 6a), the electrodeposited surfaces demonstrate over 1 order of magnitude lower CR compared to bare copper at 23 °C, and the corrosion rate of etched surfaces is about one-third of the

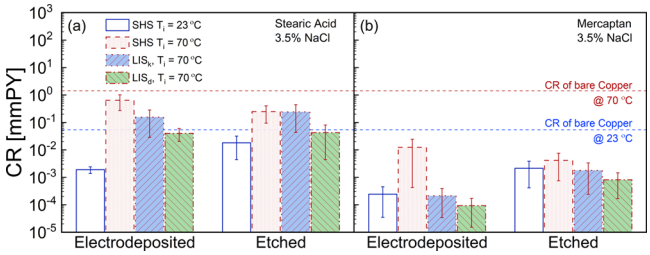

Figure 6. Comparison of CR at T_i = 23 and 70 °C for electrodeposited and etched SHSs and LISs functionalized with (a) stearic acid and (b) mercaptan for 24 h.

CR of bare surface. Among the mercaptan-functionalized SHSs (Figure 6b), the CR of electrodeposited and etched surfaces shows a reduction of over 2 decades and the CR of etched surface shows a reduction of over 1 decade at 23 °C. At the higher temperature, T_i = 70 °C, the CR values of SHSs fabricated by electrodeposition or etching are generally similar, within the experimental error bars, for both stearic acid (Figure 6a) and mercaptan (Figure 6b) functionalizations. Further, both texturing methods and both functionalization agents are seen to yield lower CR than the bare copper control sample at 70 °C. Of the two functionalization agents, mercaptan is seen to have greater temperature durability than stearic acid, as reflected in the 2 order or more reduction in CR with respect to bare copper at 70 °C (Figure 6b). In comparison, the electrodeposited and etched SHSs functionalized with stearic acid are seen to reduce the corrosion rate by 30−80% from that of the bare copper surface at 70 °C (Figure 6a).

LISs are characterized by lower corrosion rate than SHSs. Stearic acid functionalized LIS exhibits at least an order of magnitude reduced CR compared to bare copper at T_i = 70 °C (Figure 6a), whereas the corrosion rate of mercaptan-functionalized LIS is dramatically lower by about 3−4 decades (Figure 6b). With regard to texturing, stearic acid functionalized, electrodeposited LISs are seen in Figure 6a to exhibit similar anti-corrosion characteristics to their etched counterparts at high temperature. On the other hand, mercaptan-functionalized, electrodeposited LISs are characterized by distinctly lower CR compared to etched LISs, as evident from Figure 6b for both Krytox 104 and DOWSIL 510 lubricants. This is attributed to the deep asperity morphology of the electrodeposited surface, which provides a larger available volume for lubricants to wick in the interasperity spaces. Among the two lubricants, based on the average CR values, it can be seen from Figure 6a,b that the higher viscosity DOWSIL exhibits a greater corrosion resistance at higher temperature, although considering the error bars, their corrosion characteristics are relatively similar.

Overall, the results in Figure 6 depict the excellent high-temperature corrosion stability of the nonwetting surfaces fabricated in this study. Functionalization using mercaptan is seen to have greater temperature stability compared to stearic acid functionalization, with mercaptan-functionalized electrodeposited LISs demonstrating the highest corrosion resistance among all the surfaces. Accordingly, the long-term corrosion durability studies discussed in the remainder of this section focus on mercaptan-functionalized surfaces.

3.3. Long-Term Static Corrosion Durability. Corrosion durability of the surfaces immersed in a static corrosive environment over long duration was studied through a set of static immersion tests. Two SHSs (electrodeposited or etched

https://doi.org/10.1021/acs.langmuir.2c00331
Langmuir 2022, 38, 6911−6922

surfaces functionalized with mercaptan for 24 h) and four LISs (electrodeposited or etched surfaces functionalized with mercaptan for 24 h and infused with Krytox 104 or DOWSIL 510) were immersed in 3.5% NaCl solution in the annulus of the coaxial cylindrical setup (Figure 1b), along with a bare copper control sample for up to 720 h (30 days) at room temperature (T_i = 23 °C). With three replicates for each type of surface, a total of 21 coupons were studied. The coupons were removed from the solution at different time intervals and tested in fresh solution via a LP test, a nondestructive corrosion test explained in Section 2.4, from which the polarization/corrosion resistance, R_p, was calculated. A total of 252 corrosion tests were performed. The results of the long-term static corrosion tests are presented in Figure 7 as the optical microscopic images of the actual surfaces before and after the test, Figure 7a–h, and the time evolution of the corrosion resistance in Figure 7i,j, for the two texturing methods, as discussed below.

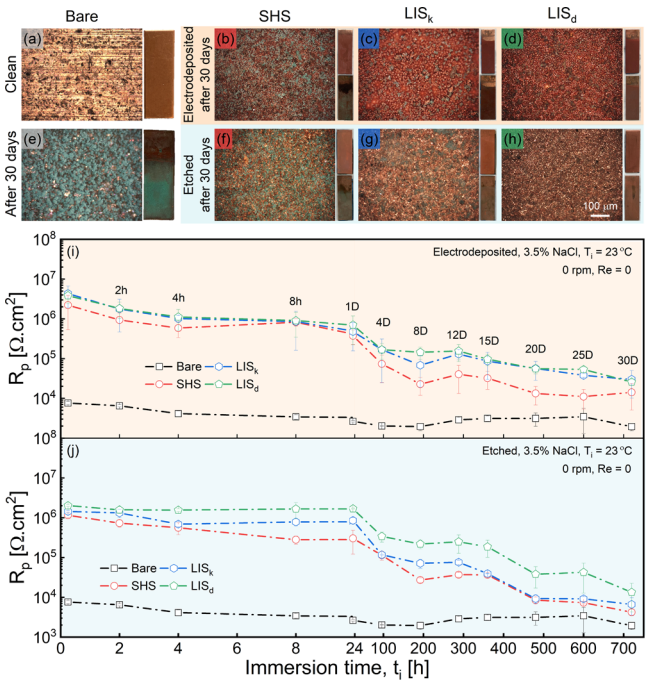

Figure 7. Optical microscopic images of (a) clean bare copper and (b–h) bare copper, SHS and LIS after 30 days of static immersion test in 3.5% NaCl solution at room temperature (T_i = 23 °C). Photographs to the right of each microscopic image are of actual 1 cm × 3 cm coupons before (top) and after (bottom) the long-term static test. Variation of polarization resistance, R_p, with immersion time, t_i, in 3.5% NaCl solution at room temperature for (i) electrodeposited and (j) etched SHS and LIS in comparison to bare copper.

Figure 7a shows the pristine smooth and clear bare copper surface before the tests. After 720 h of static immersion in the sodium chloride solution, the surface is corroded and fully covered with patina as shown in Figure 7e. Correspondingly, the polarization resistance of bare copper can be seen in Figure 7i,j to have decreased from 7.6 × 10^3 Ω·cm^2 at a 0.25 h immersion time to 1.9 × 10^3 Ω·cm^2 after 720 h of static immersion. The bare copper surface exhibits a slight increase in R_p between 24 and 288 h, which is due to the protective effect of the patina layer which eventually degrades after 480 h. The optical microscope images of the electrodeposited nonwetting surfaces, Figure 7b–d, and etched nonwetting surfaces, Figure 7f–h, after 720 h of static immersion show a significantly less visible sign of corrosion in the form of green spots in comparison to the bare copper surface in Figure 7e. Furthermore, the photographs presented to the right of the optical microscopic images are of the actual coupons before and after the long-term static immersion test, which demonstrate the degree of surface discoloration due to corrosion in the following order: bare copper > SHS > LIS$_d$ and LIS$_k$.

The qualitative observations match very well with the quantitative results in Figure 7i,j, where the polarization resistance of LIS$_k$ and LIS$_d$ is measured to be higher than that of SHS, for both texturing methods, and the corrosion resistance of all the nonwetting surfaces are 1–2 orders of magnitude greater than that of the bare control case. The Krytox 104 and DOWSIL 510 lubricated electrodeposited LIS performed almost similarly throughout the static immersion test. For the etched LIS, both types of the lubricated surfaces followed a similar trend, with DOWSIL performing slightly better, which is attributed to the higher viscosity and, in turn, greater retention of DOWSIL compared to Krytox 104. It is further noted from Figure 7i,j that the corrosion resistance of the electrodeposited SHS and LIS is greater than that for the corresponding etched nonwetting surface due to the less surface area of the shallow asperities on the etched surfaces compared to the electrodeposited surfaces. In the case of SHS, the reduced area on the etched surface translates to reduced functionalization and greater surface energy, which reduces the corrosion resistance. In the case of etched LIS, the shallow and wider asperities further result in reduced capillary forces and, in turn, less retained lubricant volume in the asperity valleys compared to the deeper/narrower asperity trenches of electrodeposited surfaces, which also lead to relatively lower corrosion resistance.

3.4. Long-Term Dynamic Corrosion Durability. Flow conditions are common in many applications, yet the long-term durability of the nonwetting surfaces exposed to the flowing corrosive environment is least explored in the literature. Flow corrosion studies were conducted using the Taylor–Couette annular flow setup described in Section 2.4. Nonwetting SHS and LIS were fabricated via the two texturing methods (electrodeposition and etching), functionalized for 24 h with mercaptan, and, in the case of LIS, infused with one of the two lubricants, Krytox 104 or DOWSIL 510. The fabricated SHS and LIS coupons along with bare copper control samples were mounted on the outer surface of the rotating drum in the Taylor–Couette flow setup (Figure 1b), in which the annulus was filled with 3.5% NaCl solution. Flow corrosion experiments were conducted at a rotation rate of 200 rpm, which yielded turbulent flow conditions with a Reynolds number of 99,000. This level of Reynolds number matches the turbulant condition in applications such as coolant flow in power plant condensers, where the Reynolds number ranges from 40,000 to 60,000.[44] The considered Reynolds number in the studies elucidates the dynamic corrosion for applications of the nonwetting surfaces to high flow rate and/or large pipe flows. Each type of surface was mounted on a separate setup to eliminate any potential adverse interactions among the different surface types.

Experiments were conducted at room temperature (T_i = 23 °C) for 720 h (30 days), with periodic removal of the samples for corrosion resistance measurements. Similar to the static tests discussed in Section 3.3, three samples for each surface

https://doi.org/10.1021/acs.langmuir.2c00331
Langmuir 2022, 38, 6911–6922

type were studied for a total of 21 coupons and 252 corrosion tests. The variation of the corrosion resistance with time for the different surfaces is summarized in Figure 8a,b for the two

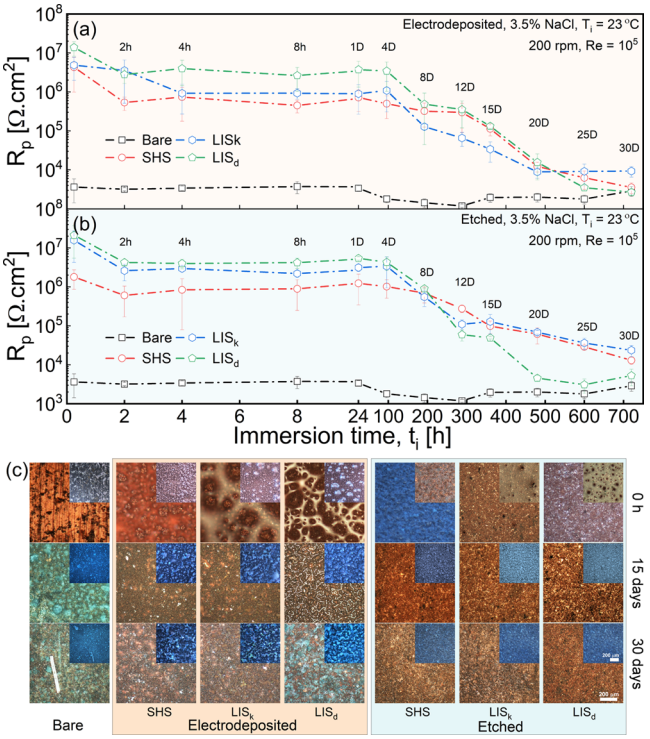

Figure 8. Variation of polarization resistance, R_p, with immersion time, t_i, in a flowing 3.5% NaCl solution at room temperature for (a) electrodeposited and (b) etched SHS and LIS in comparison to bare copper. Panel of optical microscope images of bare copper, electrodeposited SHS and LIS, and etched SHS and LIS at the start (0 h), after 15 days, and after 30 days of dynamic flow corrosion in 3.5% NaCl solution at room temperature (T_i = 23 °C). The inset images at the top right of each micrograph were taken with a fluorescent filter to elucidate the surface features.

texturing methods, along with the optical micrograph images of the surfaces at the start, in the middle, and at the end of the long-term dynamic flow experiments in Figure 8c. It can be seen from Figure 8a,b that the polarization resistance of LIS and SHS, regardless of the texturing method or infusing lubricant, exhibits three distinct regions: (1) an initial sharp decline within 2 h of immersion in the flow, (2) a relatively stable corrosion resistance between 2 and 96 h (LIS) or 288 h (SHS), and (3) a gradual decline in R_p between 96 h (LIS) or 288 h (SHS) and 720 h. The initial sharp decline is due to the shear forces of the flow rapidly eroding some of the functionalization layer as well as draining the top layers of the lubricant in the asperity valleys. Following the initial rapid deterioration, the surfaces remain stable during the second stage, causing R_p values to be nearly constant. In the third stage, the corrosion of the surfaces combined with the continued shear on the surface due to the flow causes the gradual erosion of the functionalization agent as well as further removal of the lubricant, resulting in the corrosion resistance values approaching that of bare copper.

The quantitative variation of the corrosion resistance is supported by the panel of optical microscope images in Figure 8c displaying the surfaces at the start (0 h), after 15 days, and at the end (30 days) of the experiments. The inset images in Figure 8c were taken with a fluorescent filter to better depict the transparent lubricant and other surface features. A significant morphological change is observed on the bare copper surface throughout the dynamic corrosion test. The clean smooth bare copper surface before the test was covered with a patina layer by the middle of the test, and at the end of the test, salt crystal deposition is also observed, as marked in Figure 8c. The turbulent flow condition seems to have caused slight erosion of both electrodeposited and etched SHSs, but, unlike bare copper, no visible patina layer is observed. Among the LIS, the DOWSIL-infused surfaces show a visible sign of lubricant retention on the surface, especially on the electrodeposited LIS. The deeper trenches of the electrodeposited asperities hold more infiltrated lubricant volume, and the narrower trenches correspond to larger capillary forces, both promoting lubricant retention. Further, the higher viscosity of the DOWSIL oil in contact with the larger surface area of the deeper asperity walls offers more drag resistance to drainage, leading to the greater lubricant retention. Correspondingly, the corrosion resistance values are the highest for LIS_d^D, as shown in Figure 8a. Similar to SHSs, LISs also show no or significantly less patina compared to the bare copper throughout the dynamic test.

Comparing the results from the static and dynamic corrosion tests in Figures 7 and 8, it is observed that the corrosion resistance is higher under flow conditions. The corrosion mitigation in flow can be explained by the shear force of the flow, which causes the corrosion species to be swept away from the surface, as well as the shorter residence time for corrosion to initiate. In the static condition, by the end of the 30 days, the polarization resistance of DOWSIL-infused LISs was measured to be larger or equal to that of Krytox 104-infused LISs. On the other hand, under dynamic flow, at some point during the test, the R_p value for the DOWSIL-lubricated surfaces falls below that of the Krytox 104-lubricated surfaces. Figure 8a,b shows that this crossover occurred earlier for etched cases (after 8 days of immersion) compared to electrodeposited cases (after 20 days of immersion). This trend is explained by the roughness characteristics of the surfaces and the viscosity of the lubricants. The higher the viscosity, the harder it is for a lubricant to infuse into the smaller cavities of the asperities. From the profilometer scans of the etched and electrodeposited surfaces in Figure 4c,d, it may be understood that the high-viscosity DOWSIL infuses the asperity surface well but cannot penetrate the small interspaces at the base level of the electrodeposited surface. However, its higher viscosity helps withstand the shear forces of the flow, causing increased lubricant retention in the top layers and corrosion protection. On the other hand, the lower viscosity Krytox 104 is able to better infiltrate into the base level of the asperities but cannot withstand the shear forces of the flow as well as the higher viscosity DOWSIL. By the end of the dynamic test, therefore, the strong shear force has swept the lubricant from the top level of the asperities but the strong capillary force deeper in the asperities locks in any lubricant that is able to penetrate to the depths of the asperity valleys. Since lower viscosity Krytox 104 is able to reach the base of the asperities better than the higher viscosity DOWSIL, LIS_k ends up with a higher corrosion resistance than LIS_d over longer term immersion, as can be seen at 30 days in Figure 8a,b. The earlier crossover for the etched LIS compared to the electrodeposited LIS is due to the higher roughness of the latter, which can accommodate a larger volume of the lubricant

https://doi.org/10.1021/acs.langmuir.2c00331
Langmuir 2022, 38, 6911−6922

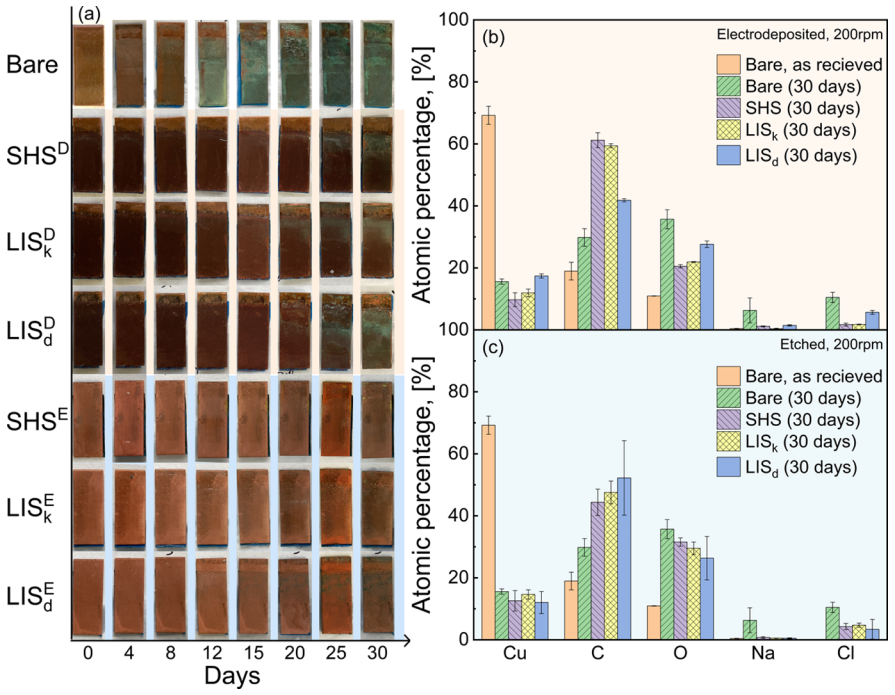

Figure 9. (a) Panel of photographs of the actual 1 cm × 3 cm coupons taken at different times throughout the long-term dynamic corrosion tests. The top 1 cm in each coupon was used for handling purposes and the bottom 1 cm was used in corrosion measurements. EDX elemental composition analysis of (b) electrodeposited and (c) etched SHS and LIS along with bare copper after the dynamic flow corrosion test in 3.5% NaCl solution.

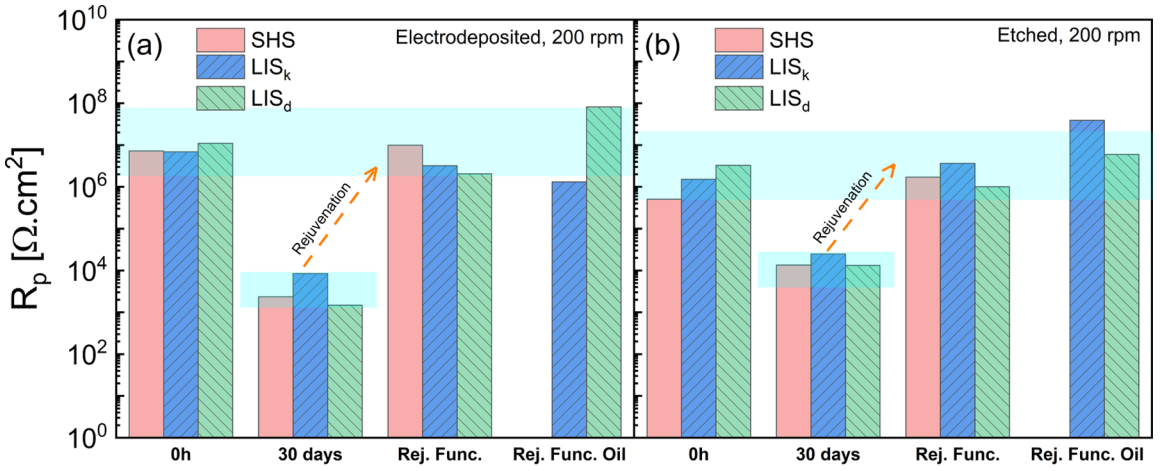

Figure 10. Polarization resistance, R_p, for (a) electrodeposited and (b) etched surfaces before dynamic corrosion test (0 h), after dynamic corrosion test (30 days), after rejuvenation with mercaptan functionalization, and after rejuvenation via functionalization and lubricant infusion. The light blue shading denotes the range of the error bars in the measured corrosion resistance values at 0 h.

at the top level of the asperity valleys. Thus, LIS_d^E loses DOWSIL quicker than LIS_d^D, leading to a sooner decrease of the corrosion resistance below that of LIS_k^E, which has deeper penetration of the lower viscosity Krytox 104 in the asperities.

Overall, Figure 8 reveals that the corrosion resistance values of the nonwetting surfaces are slightly better than or similar to the bare copper surface at the end of the long-term dynamic corrosion test. The appearance of the actual coupon surfaces after 30 days of dynamic flow corrosion, presented in Figure 9a, shows significant discoloration of the bare copper, a sign of corrosion and patina layer formation, which is not observed for the modified surfaces in the same panel of photographs. To further quantify this difference, elemental composition of the coupons was examined via EDX analysis, and the results are presented in Figure 9b,c for the electrodeposited and etched coupons, respectively. The elemental analysis results in both figures show the presence of a significantly higher amount of sodium and chlorine on the bare copper surface (green bars) compared to all the nonwetting surfaces after 30 days of dynamic corrosion test. Moreover, a smaller amount of copper was detected for the bare copper surface after 30 days compared to the elemental copper detected before the test, which asserts the presence of a thick patina layer. This layer protects against corrosion for bare copper surfaces as was quantitatively revealed itself in the R_p values presented in Figure 8.

3.5. Rejuvenation. The results of the long-term static and dynamic flow tests presented in Figures 7 and 8 show that even

https://doi.org/10.1021/acs.langmuir.2c00331
Langmuir 2022, 38, 6911−6922

though the modified surfaces (SHS and LIS) degrade in their corrosion resistance over time, they all retain better corrosion inhibition characteristics than bare copper, have much less corrosive compounds on their surfaces and, importantly, preserve their multiscale texture. This suggests that the nonwetting SHS and LIS may be rejuvenated by re-functionalization (for SHS) and, further, lubricant re-infusion (for LIS), without the need for surface re-texturing. Figure 10 shows that the electrodeposited and etched nonwetting surfaces had an average corrosion resistance of about 8 and 2 MΩ·cm^2, respectively, prior to the long-term corrosion study. After the 30 day dynamic flow corrosion test at 200 rpm (Reynolds number ≈ 99,000), the polarization resistance decreased to about 0.004 and 0.017 MΩ·cm^2 for electrodeposited and etched nonwetting surfaces, respectively.

After rejuvenation by immersion in mercaptan solution for 6 h, the nonwetting characteristics of the surfaces were revived to be superhydrophobic (CA above 150° and roll-off angle below 10°), resulting in an average polarization resistance of 5 and 2 MΩ·cm^2, respectively, for the electrodeposited and etched surfaces, as can be seen in Figure 10a,b. The revived corrosion resistance matches with the initial corrosion resistance of the surfaces prior to the long-term corrosion test. After re-functionalization, the coupons that were lubricant-infused before the dynamic corrosion test were re-infused with either Krytox 104 or DOWSIL 510, which resulted in the full restoration of their nonwetting properties (sliding angle below 10°), and average polarization resistances of 41 and 22 MΩ·cm^2 were measured for the rejuvenated electrodeposited and etched LISs, respectively. The study demonstrates successful rejuvenation of the surfaces and revival of the excellent anti-corrosion properties of the superhydrophobic and lubricant-infused copper surfaces.

Collectively, this section presented evidence, for the first time, of the long-term corrosion robustness of the fabricated nonwetting surfaces in static, dynamic, and high-temperature corrosion environments. The primary focus of this article was on facile fabrication and study of the morphology, wettability, and corrosion performance of copper surfaces under static as well as dynamic flow conditions. Through the study, it was seen that the surface roughness profiles resulting from the texturing plays an important role in balancing lubricant infiltration and retention in service. The results in this section may be used to deduce general pathways for selection of corrosion-resistant copper surfaces based on applications. For higher temperature applications, mercaptan functionalization is the recommended choice, while at lower temperatures, the stearic acid functionalization agent works equally well. In applications where possible contamination with oil is not an issue, LISs may be used for their higher corrosion resistance over SHSs. A dedicated study on optimizing surface roughness features and lubricant properties for corrosion protection may be conducted in a future study.

4. CONCLUSIONS

A multiparametric study was presented on the effects of nonwetting surface fabrication methods, functionalizing agents, infused lubricants, corrosion solution temperature, and corrosion conditions (static vis-à-vis dynamic) on the long-term corrosion characteristics in 3.5% NaCl solution. Overall, the study encompassed over 650 measurements on 90 coupons, from which the major findings are as follows: SHS and LIS functionalized with mercaptan showed at least 1 order of magnitude improved corrosion resistance at 70 °C compared to stearic acid and 2−3 decades lower corrosion rate compared to bare copper. Mercaptan-functionalized electrodeposited LIS exhibited the least corrosion among all the surfaces at the high temperature. Both Krytox 104 and DOWSIL 510 were equally effective as lubricants in the high-temperature corrosion resistance of LISs. In extended period corrosion studies, LISs infused with DOWSIL 510 or Krytox 104, alike, showed superior corrosion resistance to SHS, and both SHSs and LISs performed significantly better than bare copper throughout the long-term static corrosion test. Between the two texturing methods, electrodeposited nonwetting surfaces, by virtue of the deeper and narrower asperity trenches to hold lubricant as well as the greater asperity surface area for functionalization, were more corrosion resistant than etched nonwetting surfaces. Both SHSs and LISs, despite experiencing harshest corrosion environments for long duration, were shown to rejuvenate excellently and regain their original corrosion inhibition properties.

For the first time, the results of this study shed light on the interactions among the various aspects of fabrication of nonwetting surfaces, including texturing methods, functionalization agents, and lubricant types, on the high temperature and long-term corrosion durability of the surfaces. This study paves the way for selection of proper parameters for the fabrication of nonwetting surfaces for the application of interest.

AUTHOR INFORMATION

Corresponding Author

R. Pitchumani − *Advanced Materials and Technologies Laboratory, Department of Mechanical Engineering, Virginia Tech, Blacksburg, Virginia 24061-0238, United States;* orcid.org/0000-0001-9565-1639; Phone: +1 703 538 3772; Email: pitchu@vt.edu

Author

S.M.A. Mousavi − *Advanced Materials and Technologies Laboratory, Department of Mechanical Engineering, Virginia Tech, Blacksburg, Virginia 24061-0238, United States*

Complete contact information is available at: https://pubs.acs.org/10.1021/acs.langmuir.2c00331

Notes

The authors declare no competing financial interest.

ACKNOWLEDGMENTS

The material reported in this publication is based on the work supported by the U.S. Department of Energy under the award no DE-FE0031556. This publication was prepared as an account of work sponsored by an agency of the United States Government. Neither the United States Government nor any agency thereof, nor any of their employees, makes any warranty, express or implied, or assumes any legal liability or responsibility for the accuracy, completeness, or usefulness of any information, apparatus, product, or process disclosed, or represents that its use would not infringe on privately owned rights. Reference herein to any specific commercial product, process, or service by trade name, trademark, manufacturer, or otherwise does not necessarily constitute or imply its endorsement, recommendation, or favoring by the United States Government or any agency thereof. The views and opinions of authors expressed herein do not necessarily state or

reflect those of the United States Government or any agency thereof.

REFERENCES

(1) Law, K.; Zhao, H. *Surface Wetting: Characterization, Contact Angle, and Fundamentals*; Springer, 2016.

(2) Ramanujam Padmavathi, A.; Sriyutha Murthy, P.; Das, A.; Subba Rao, T. Enhanced Antifouling Property of Polydimethylsiloxane-CuO Nanocomposite in Marine Environment. *Mater. Lett.* **2021**, *301*, 130342.

(3) Liu, M.; Li, S.; Wang, H.; Jiang, R.; Zhou, X. Research Progress of Environmentally Friendly Marine Antifouling Coatings. *Polym. Chem.* **2021**, *12*, 3702−3720.

(4) Guo, W.; Li, Z.; Ma, Z. Review of Non-Fluorinated Durable Water Repellent and Stain-Resistant Materials and Their Future Development. *J. Phys. Conf.* **2021**, *1904*, 012010.

(5) Ou, J.; Wang, F.; Li, W.; Yan, M.; Amirfazli, A. Methyltrimethoxysilane as a Multipurpose Chemical for Durable Superhydrophobic Cotton Fabric. *Prog. Org. Coating* **2020**, *146*, 105700.

(6) Belhadjamor, M.; Mansori, M.; Belghith, S.; Mezlini, S. Anti-Fingerprint Properties of Engineering Surfaces: A Review. *Taylor Francis* **2016**, *34*, 85−120.

(7) Piscitelli, F.; Tescione, F.; Mazzola, L.; Bruno, G.; Lavorgna, M. On a Simplified Method to Produce Hydrophobic Coatings for Aeronautical Applications. *Appl. Surf. Sci.* **2019**, *472*, 71−81.

(8) Tesler, A. B.; Kim, P.; Kolle, S.; Howell, C.; Ahanotu, O.; Aizenberg, J. Extremely Durable Biofouling-Resistant Metallic Surfaces Based on Electrodeposited Nanoporous Tungstite Films on Steel. *Nat. Commun.* **2015**, *6*, 8649.

(9) Ivanovich, U. A.; Popova, T. N.; Viktorovich, K. A. The Effect of the Loss of Superhydrophobic Surface Properties on Biofouling and Flow around Shipbuilding's Steel Plates. *Ocean. Eng.* **2020**, *214*, 107801.

(10) Masoudi, A.; Irajizad, P.; Farokhnia, N.; Kashyap, V.; Ghasemi, H. Antiscaling Magnetic Slippery Surfaces. *ACS Appl. Mater. Interfaces* **2017**, *9*, 21025−21033.

(11) Zhu, Y.; Li, H.; Zhu, M.; Wang, H.; Li, Z. Dynamic and Active Antiscaling via Scale Inhibitor Pre-Stored Superhydrophobic Coating. *Chem. Eng. J.* **2021**, *403*, 126467.

(12) Mousavi, S. M. A.; Pitchumani, R. A Study of Corrosion on Electrodeposited Superhydrophobic Copper Surfaces. *Corros. Sci.* **2021**, *186*, 109420.

(13) Cui, M.; Wang, B.; Wang, Z. Nature-Inspired Strategy for Anticorrosion. *Adv. Eng. Mater.* **2019**, *21*, 1801379.

(14) Xu, J.; Cai, Q.; Lian, Z.; Yu, Z.; Ren, W.; Yu, H. Research Progress on Corrosion Resistance of Magnesium Alloys with Bio-Inspired Water-Repellent Properties: A Review. *J. Bionic Eng.* **2021**, *18*, 735−763.

(15) Mousavi, S. M. A.; Pitchumani, R. Bioinspired Nonwetting Surfaces for Corrosion Inhibition over a Range of Temperature and Corrosivity. *J. Colloid Interface Sci.* **2022**, *607*, 323−333.

(16) Hou, B.; Li, X.; Ma, X.; Du, C.; Zhang, D.; Zheng, M.; Xu, W.; Lu, D.; Ma, F. The Cost of Corrosion in China. *npj Mater. Degrad.* **2017**, *1*, 4.

(17) Kruger, J. Cost of Metallic Corrosion. *Uhlig's Corrosion Handbook*; 2nd ed., Revie, R. W., Ed.; Wiley: New York, 2011; Chapter 2, pp 15−20.

(18) Khodakarami, S.; Zhao, H.; Rabbi, K. F.; Miljkovic, N. Scalable Corrosion-Resistant Coatings for Thermal Applications. *ACS Appl. Mater. Interfaces* **2021**, *13*, 4519−4534.

(19) Latthe, S. S.; Sutar, R. S.; Bhosale, A. K.; Nagappan, S.; Ha, C.-S.; Sadasivuni, K. K.; Liu, S.; Xing, R. Recent Developments in Air-Trapped Superhydrophobic and Liquid-Infused Slippery Surfaces for Anti-Icing Application. *Prog. Org. Coating* **2019**, *137*, 105373.

(20) Wang, P.; Lu, Z.; Zhang, D. Slippery Liquid-Infused Porous Surfaces Fabricated on Aluminum as a Barrier to Corrosion Induced by Sulfate Reducing Bacteria. *Corros. Sci.* **2015**, *93*, 159−166.

(21) Song, T.; Liu, Q.; Liu, J.; Yang, W.; Chen, R.; Jing, X.; Takahashi, K.; Wang, J. Fabrication of Super Slippery Sheet-Layered and Porous Anodic Aluminium Oxide Surfaces and Its Anticorrosion Property. *Appl. Surf. Sci.* **2015**, *355*, 495−501.

(22) Shi, Z.; Xiao, Y.; Qiu, R.; Niu, S.; Wang, P. A Facile and Mild Route for Fabricating Slippery Liquid-Infused Porous Surface (SLIPS) on CuZn with Corrosion Resistance and Self-Healing Properties. *Surf. Coating. Technol.* **2017**, *330*, 102−112.

(23) Xiang, T.; Zhang, M.; Sadig, H. R.; Li, Z.; Zhang, M.; Dong, C.; Yang, L.; Chan, W.; Li, C. Slippery Liquid-Infused Porous Surface for Corrosion Protection with Self-Healing Property. *Chem. Eng. J.* **2018**, *345*, 147−155.

(24) Qiu, R.; Zhang, Q.; Wang, P.; Jiang, L.; Hou, J.; Guo, W.; Zhang, H. Fabrication of Slippery Liquid-Infused Porous Surface Based on Carbon Fiber with Enhanced Corrosion Inhibition Property. *Colloids Surf., A* **2014**, *453*, 132−141.

(25) Villegas, M.; Zhang, Y.; Jarad, N. A.; Soleymani, L.; Didar, T. F. Liquid-Infused Surfaces: A Review of Theory, Design, and Applications. *ACS Nano* **2019**, *13*, 8517−8536.

(26) Liu, J.; Fang, X.; Zhu, C.; Xing, X.; Cui, G.; Li, Z. Fabrication of Superhydrophobic Coatings for Corrosion Protection by Electrodeposition: A Comprehensive Review. *Colloids Surf., A* **2020**, *607*, 125498.

(27) Howell, C.; Grinthal, A.; Sunny, S.; Aizenberg, M.; Aizenberg, J. Designing Liquid-Infused Surfaces for Medical Applications: A Review. *Adv. Mater.* **2018**, *30*, 1802724.

(28) Zhang, X.-X.; Cai, S.; You, D.; Yan, L.-H.; Lv, H.-B.; Yuan, X.-D.; Jiang, B. Template-Free Sol-Gel Preparation of Superhydrophobic ORMOSIL Films for Double-Wavelength Broadband Antireflective Coatings. *Adv. Funct. Mater.* **2013**, *23*, 4361−4365.

(29) Lee, S.; Kim, B.; Kim, S.-H.; Kim, E.; Jang, J.-H. Superhydrophobic, Reversibly Elastic, Moldable, and Electrospun (SupREME) Fibers with Multimodal Functions: From Oil Absorbents to Local Drug Delivery Adjuvants. *Adv. Funct. Mater.* **2017**, *27*, 1702310.

(30) Emelyanenko, K. A.; Sanzharovsky, N. A.; Chulkova, E. V.; Ganne, A. A.; Emelyanenko, A. M.; Boinovich, L. B. Superhydrophobic Corrosion Resistant Coatings for Copper via IR Nanosecond Laser Processing. *Mater. Res. Express* **2018**, *5*, 115001.

(31) Wan, Y.; Chen, M.; Liu, W.; Shen, X.; Min, Y.; Xu, Q. The Research on Preparation of Superhydrophobic Surfaces of Pure Copper by Hydrothermal Method and Its Corrosion Resistance. *Electrochim. Acta* **2018**, *270*, 310−318.

(32) Dimitrakellis, P.; Ellinas, K.; Kaprou, G. D.; Mastellos, D. C.; Tserepi, A.; Gogolides, E. Bactericidal Action of Smooth and Plasma Micro-Nanotextured Polymeric Surfaces with Varying Wettability, Enhanced by Incorporation of a Biocidal Agent. *Macromol. Mater. Eng.* **2021**, *306*, 2000694.

(33) He, Z.; Zeng, Y.; Zhou, M.; Min, Y.; Shen, X.; Xu, Q. Superhydrophobic Films with Enhanced Corrosion Resistance and Self-Cleaning Performance on an Al Alloy. *Langmuir* **2021**, *37*, 524−541.

(34) Peppou-Chapman, S.; Hong, J. K.; Waterhouse, A.; Neto, C. Life and Death of Liquid-Infused Surfaces: A Review on the Choice, Analysis and Fate of the Infused Liquid Layer. *Chem. Soc. Rev.* **2020**, *49*, 3688.

(35) Wang, Y.; Zhou, X.; Yin, M.; Pu, J.; Yuan, N.; Ding, J. Superhydrophobic and Self-Healing Mg-Al Layered Double Hydroxide/Silane Composite Coatings on the Mg Alloy Surface with a Long-Term Anti-Corrosion Lifetime. *Langmuir* **2021**, *37*, 8129−8138.

(36) Zhang, J.; Wei, J.; Li, B.; Zhao, X.; Zhang, J. Long-Term Corrosion Protection for Magnesium Alloy by Two-Layer Self-Healing Superamphiphobic Coatings Based on Shape Memory Polymers and Attapulgite. *J. Colloid Interface Sci.* **2021**, *594*, 836−847.

(37) Boinovich, L. B.; Emelyanenko, K. A.; Domantovsky, A. G.; Chulkova, E. V.; Shiryaev, A. A.; Emelyanenko, A. M. Pulsed Laser Induced Triple Layer Copper Oxide Structure for Durable Polyfunctionality of Superhydrophobic Coatings. *Adv. Mater. Interfac.* **2018**, *5*, 1801099.

https://doi.org/10.1021/acs.langmuir.2c00331
Langmuir 2022, 38, 6911−6922

(38) Wexler, J. S.; Jacobi, I.; Stone, H. A. Shear-Driven Failure of Liquid-Infused Surfaces. *Phys. Rev. Lett.* **2015**, *114*, 168301.
(39) Quan, Y.-Y.; Chen, Z.; Lai, Y.; Huang, Z.-S.; Li, H. Recent Advances in Fabricating Durable Superhydrophobic Surfaces: A Review in the Aspects of Structures and Materials. *Mater. Chem. Front.* **2021**, *5*, 1655−1682.
(40) Mousavi, S. M. A.; Pitchumani, R. Temperature-Dependent Dynamic Fouling on Superhydrophobic and Slippery Nonwetting Copper Surfaces. *Chem. Eng. J.* **2022**, *431*, 133960.
(41) ASTM International. *Standard Practice for Conventions Applicable to Electrochemical Measurements in Corrosion Testing*, 2019. ASTM G3-14.
(42) Jain, R.; Pitchumani, R. Fractal Model for Wettability of Rough Surfaces. *Langmuir* **2017**, *33*, 7181−7190.
(43) Hatte, S.; Pitchumani, R. Analysis of Convection Heat Transfer on Multiscale Rough Superhydrophobic and Liquid Infused Surfaces. *Chem. Eng. J.* **2021**, *424*, 130256.
(44) Nithyanandam, K.; Shoaei, P.; Pitchumani, R. Technoeconomic Analysis of Thermoelectric Power Plant Condensers with Nonwetting Surfaces. *Energy* **2021**, *227*, 120450.

https://doi.org/10.1021/acs.langmuir.2c00331
Langmuir 2022, 38, 6911−6922